Impact of Silver Ions Doping and Calcination on the Physicochemical Characteristics of TiO_2 Nanoparticles with Photocatalytic and Regeneration Potential

Saqib, Najm Us•; Adnan, Rohana*+

School of Chemical Sciences, Universiti Sains Malaysia, 11800 Penang, MALAYSIA

Shah, Irfan

Department of Chemistry, The University of Lahore, Sargodha Campus, PAKISTAN

ABSTRACT: *Visible light-driven Ag^+ doped TiO_2 photocatalysts were successfully prepared with modified low-cost Liquid Impregnation (LI) method yielding up to 95 % product. The native and newly synthesized photocatalysts were calcined at various temperatures and characterized using diffused reflectance spectroscopy (UV/Vis-DRS), XRD, XPS, TEM, EDX, XRF, and pH_{PZC} analyses. The XRD results for all samples revealed that the anatase phase was dominant at all calcination temperatures. The Ag^+ doping reduced the bandgap energy to 2.88 eV, which significantly enhanced the photocatalytic efficiency towards Methylene Blue (MB) under compact fluorescent light. The photocatalytic efficacy of the nano-catalysts was also tested using a binary solution containing a model dye (MB) and Cd^{2+} under ordinary compact fluorescent light. The presence of competitive ions i.e. Cd^{2+} increased the MB degradation up to 4 folds under the ambient conditions whereby the maximum amount of MB adsorbed by nano-catalysts reached 46 mg/g. The high-temperature combustion method was found more effective for the regeneration of TiO_2 photocatalysts compared to the chemical regeneration. The reusable character of the regenerated samples posed a significant impact on the current work to be applied in wastewater treatment in bulk.*

KEYWORDS: *Titanium dioxide; Doping; Degradation; Photocatalysis; Regeneration*.

INTRODUCTION

Textile industries are one of the major contributors to industrial water pollution. Above 10,000 different dyes and pigments used in industries generate over 0.7 million tons of dyes waste annually [1]. Dyes are generally recalcitrant and remain unattended due to their non-biodegradable nature and high stability against light, temperature, chemicals, detergents, and water [1,2]. It has been reported that the textile industry contributes up to 200,000 tons of dyes effluents annually as a result of inefficient dyeing processes [1]. The colored wastewater

***** *To whom correspondence should be addressed.*
+ E-mail: r_adnan@usm.my
Other Address: Department of Chemistry, University of Buner, Buner, PAKISTAN
1021-9986/2021/4/1012-1022 11/$/6.01

not only affects the water transparency by absorbing the incident light radiations but also pose a toxic and carcinogenic impact on humans and other animals [2]. Among various hazardous pollutants other than dyes, cadmium (Cd^{2+}) is has been found severely toxic causing serious harm to the vital organs such as damaging liver, kidney tissue, and brain even at very low concentrations [3, 4]. Due to the adverse effects at trace levels, World Health Organization (WHO) drinking water Threshold Limit Values (TLV) for cadmium have been set to 0.005 mg/L [5]. Out of many cadmium removal techniques, adsorption has been considered the best and highly effective removal method to overcome the toxic sludge disposal issues [3, 4].

Titanium dioxide (TiO_2), a highly efficient photocatalyst, is widely used in the advanced oxidation processes (AOP) of wastewater treatment [6]. More often, TiO_2 is used in the heterogeneous photocatalysis of dyes due to its high degradation and adsorption efficiencies and environmentally friendly nature [7-9]. The other interesting features of TiO_2 photocatalyst include highly oxidizing photo-generated electron-hole pair, chemical stability, low toxicity, and high photo-stability [10]. Although TiO_2 is capable of high efficacy the high bandgap energy limits the potential photocatalytic application of anatase phase to UV light ($\lambda < 387$ nm) which is only 5% of the sunlight [10]. Therefore, it is *crucial* to modify the surface of TiO_2 for better photocatalytic applications to efficiently harness the sunlight energy and shift the photo-response of photocatalyst into the visible light region [7]. In order to improve the working range of TiO_2 photocatalysts, various modifications pathways have been routed to maximize the use of available visible solar light. These modifications include doping with metals and non-metals [11-14], dye sensitization [15], and coupling with the low bandgap semiconductors [16].

The present study is thus focused on one such surface modification technique where Ag^+ doped TiO_2 photocatalyst were prepared by following a slightly modified Liquid Impregnation (LI) method using low-cost amorphous titanium (IV) oxide precursor. The advantageous aspect of the LI approach is the uniform deposition of silver on TiO_2 .urface as Ag^+ ions which absorb electrons during photocatalysis and thus reduces the electron/hole pair recombination rate. Also, this study corroborates the influence of different calcination temperatures, its effect on reducing the bandgap, and its impact on the other surface properties of undoped and Ag-doped TiO_2. Generally, the wastewaters contain high salt concentrations and the effect of counter ions i.e. ionic strength of the interfering ions is important to get attended in dyes removal. Meanwhile, the presence of competitive metal ions (M^{n+}) has been reported to enhance the degradation efficiency of dye by reducing the photo-generated electron-hole pair recombination rate [17]. In this work, the removal efficiencies of all the prepared samples were tested in the binary solutions of dye, Methylene Blue (MB), and metal ions, Cd^{2+} under normal lab conditions.

EXPERIMENTAL SECTION

Materials

General Purpose Reagent (GPR) titanium (IV) oxide (amorphous) was purchased from Sigma-Aldrich, while silver nitrate salt was obtained from R & M Chemicals. Furthermore, HNO_3, NaOH, $NaNO_3$, and Methylene Blue ($C_{16}H_{18}ClN_3$) were received from QRec Asia. All chemicals were of analytical grade and were used without further purification.

Preparation of pure and Ag/TiO_2 nanoparticles

Pure and Ag-doped TiO_2 nanoparticles were prepared by the liquid impregnation (LI) method reported in the literature with slight modifications [18]. Firstly, 0.065 g $AgNO_3$ was added to 100 mL deionized water and kept the Ag ion concentration at a 1% mole ratio with respect to the substrate, TiO_2. Then, 3 g GPR TiO_2 was slowly added to it and the mixture was agitated on a magnetic stirrer (model DAIHAN WiseStirr) at a stirring rate of 350 rpm, continuously for 12 h, and then allowed to settle for another 12 h. Finally, the slurry was dried in an oven for 12 h at 105 °C and the dried samples were ground and calcined at different temperatures i.e. 500 and 700 °C for 3 h in a furnace. Pure TiO_2 nanoparticles were also prepared using the same method in the absence of metal dopants.

The percent yield of doped and pure TiO_2 using LI method with GPR titanium (IV) oxide precursor was up to 95 %, calculated by using the following equation:

$$\text{Percent yield (\%)} = \frac{\text{Actual yield}}{\text{Theoretical yield}} \times 100 \quad (1)$$

Characterizations

Powder X-ray diffraction technique was used to study the crystalline phase and crystallite size of the prepared nanoparticles. XRD patterns were obtained using PANalytical X'Pert PRO MRD PW3040, with Cu-K_α radiation at 2θ angle ranging from 20° to 80°. The crystallites size was determined from the X-ray diffraction patterns based on the Debye-Scherrer equation [19]:

$$D = \frac{k\lambda}{\beta \cos\theta} \quad (2)$$

Where k is the shape factor and is equal to 0.9, λ is the radiation wavelength (1.54 Å), β is the full width of a diffraction line at one-half of maximum intensity in radians. The internal surface morphology of the prepared nanoparticles was studied by the Transmission Electron Microscopy (TEM) using a Philips CM12 instrument. The diffused reflectance of pure and Ag-doped TiO_2 samples were analyzed by using UV/Vis spectrophotometer, model CARY 5000 UV/VIS/NIR whereby the electronic properties of the nanoparticles were investigated by using the remission function of Kubelka-Munk, (R) [20].

$$F(R_\infty) = \frac{(1 - R_\infty)}{2R_\infty} \quad (3)$$

Determination of the pH of point of zero charge (pH_{PZC})

The pH_{PZC} of pure and Ag ion-doped TiO_2 nanoparticles were determined by pH drift method [21]. A series of 0.1 M $NaNO_3$ solutions were prepared and the initial pHs were adjusted in the range of 2 to 12 by dropwise addition of either 0.01-0.1 M HNO_3 or NaOH solutions. To each solution, 0.1 g samples were added subsequently and equilibrated for 24 h. The final pH of each suspension was noted and the difference between initial and final pH (ΔpH) was plotted against the initial pH. The point, at which the curve crosses zero, was taken as the pH_{PZC} of the material.

Photocatalytic activity test

All the photocatalytic experiments were conducted with optimized dose amount (0.2 g), pH (6.8±0.1), stirring speed (250 rpm), contact time (3 h), and under normal conditions by using ordinary compact fluorescent light. The photocatalytic degradation efficiency (E %) of pure and Ag-doped TiO_2 samples were measured by using the following equation:

$$E(\%) = \frac{C_\circ - C_f}{C_\circ} \times 100 \quad (4)$$

Where C_o and C_f are the initial and final concentrations of MB (mg/L) in an aqueous solution, respectively. As much as 0.2 g of nanoparticles was mixed with 80 mL of 30 mg/L MB solution in 250 mL flasks separately. The suspensions were stirred on an orbital shaker (model IKA Basic 260) for 3 h at a stirring speed of 250 rpm. After equilibration, the suspensions were centrifuged at 5000 rpm for 5 min to separate the nanoparticles while the supernatant was analyzed for the remaining concentration of MB at the wavelength (λ) = 660 nm using a Shimadzu 2600, UV-Vis spectrophotometer.

On the other hand, Cd^{2+} ion solutions were added to MB solution and again the photocatalytic degradation investigations were performed for all the prepared NanoParticles (NPs) under normal conditions of pH, room temperature and using compact fluorescent light. The Cd^{2+} ion and MB concentrations were kept 200 mg/L.

Elemental analysis of fresh and spent, pure, and Ag-doped TiO_2, was conducted by using Energy Dispersion X-ray (EDX) spectroscopy (model Oxford instrument X-Max 50 mm^2) and X-Ray Fluorescence (XRF) spectrometer (model ZSX Primus II, Rigaku).

Regeneration of photocatalyst

Regeneration ability of the used photocatalysts was examined via high-temperature combustion and Fenton oxidation methods with slight modifications [22]. In physical regeneration of the used photocatalysts, the samples collected were exposed to high calcination temperature treatment (530±20 °C) in a furnace with a heating rate of 5 °C/min for 3 h. For Fenton oxidation, $Fe(NO_3)_3.9H_2O/H_2O_2$ solutions were prepared with iron (Fe) concentrations of 10^{-2} M and 3 % H_2O_2. The spent photocatalysts samples were mixed with $Fe(NO_3)_3.9H_2O/H_2O_2$ solution at ambient temperature for 8 h and then washed with distilled water three times. After washing, all the samples were centrifuged at 5000 rpm for 5 min and dried in an oven at 70 ^oC. The reusability of each sample was investigated up to three cycles upon continuous use.

RESULTS AND DISCUSSIONS

XRD Analysis

X-ray diffraction technique was used to investigate the crystallite size and the crystal phase composition of pure and Ag^+ doped TiO_2 nanoparticles. The samples calcined at different temperatures i.e. 500 and 700 °C depicted with dominant anatase phase (JCPDS 84-1286) [23], as shown in Fig. 1. The crystallites sizes at different calcination temperatures were calculated using the Scherrer equation for the anatase (1 0 1) peak and the average particle size values are given in Table 1. All the samples were annealed at above 400 °C which was found advantageous in producing pure anatase phase.

Since the ionic radius of Ag^+ ion (126 pm) is larger than Ti^{+4} ion (68 pm), the dopants Ag^+ cannot diffuse into the TiO_2 lattice [24]. Hence, it can be inferred that the addition of Ag^+ in smaller concentrations (in this case 1 M %) is unable to alter the TiO_2 lattice phase composition, neither by changing the position nor the width of the peak. Previously, *Li et al.* [25] reported that the addition of Ag dopant increases the density of surface defects and oxygen vacancies concentration of anatase phase which favors anatase to rutile transformation when the amount of Ag dopant increased to 2 wt.%. In the present study, XRD results showed that pure TiO_2 samples were in the anatase phase at all the calcination temperatures except for the sample calcined at 700 °C which contains 1.30 % rutile phase.

The average particles size of pure samples increased with the increase in calcination temperature; however, the effect was less obvious for the doped samples. Upon increasing the calcination temperatures from 500 to 700 °C, more intense and sharper anatase (1 0 1) peaks were produced demonstrating improved crystallinity for the samples. The results are also consistent with the reduction in anatase particles size (from 55.48 to 50.82 nm) for Ag-doped TiO_2 (Table 1). As reported earlier by *Ahmad et al*. [26], the decrease in anatase particles size is due to the Ag^+ doping which increased the specific surface area of particles as well as surface defects on the surface of Ag^+ doped TiO_2.

TEM Analysis

TEM studies were conducted to investigate the internal morphology and effect of metal doping on the surface morphology of Ag^+ doped TiO_2 samples. The selected

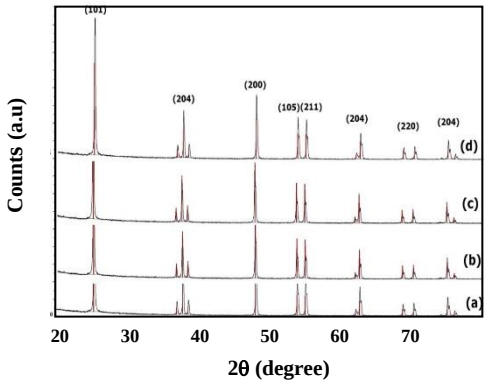

Fig. 1: XRD patterns of TiO_2 at different calcination temperatures (a) 500 °C (b) 700 °C and Ag^+ doped TiO_2 (c) 500 °C (d) 700 °C, respectively.

micrographs of pure and Ag-doped TiO_2 at different calcination temperatures are shown in Fig. 2.

It can be observed from TEM micrographs that, calcination temperature showed no significant effect on the surface morphology of pure TiO_2. For doped samples, the metal deposits were in a spherical shape and homogeneously dispersed on the surface of TiO_2. The particle size of TiO_2 (60-90 nm) measured through TEM was found larger than the particle size calculated from the Scherrer equation which can be due to the presence of agglomerates formed as a result of the high surface energy of the TiO_2 particles [27]. Overall, calcination temperatures posed a discrete effect on the particle size. A more uniform distribution of deposited Ag particles (which appeared as black color dots) was observed in Ag/TiO_2 samples calcined at 500 °C. It is believed that, the homogeneous distribution of deposited metal dopant is responsible for the reduction in bandgap and enhanced photocatalytic activity of Ag/TiO_2 calcined at 500 °C as compared to the Ag^+ doped sample calcined at the higher temperature.

Diffused Reflectance (DR) UV-Visible spectroscopic analysis

The DR UV-Vis results of pure and Ag^+ doped TiO_2 nanoparticles showed the highest absorption in UV region (Fig. 3). In comparison with pure TiO_2 samples, the DR UV-Vis spectra of Ag^+ doped TiO_2 revealed a shift in the absorption edge to longer wavelength. Thus, it can be augmented that, Ag ion doping significantly increased the absorption in the visible region (redshift). The bandgap

Table 1:Particle size and anatase phase percentage of pure and Ag^+ doped TiO_2 nanoparticles prepared at different calcination temperatures

Samples	Calcination temperature (°C)	Particle size (nm) (1 0 1) peak	Average particle size (nm)	Anatase phase (%)	Direct band gap (eV)	Indirect band gap (eV)	pH_{PZC}
TiO_2	500	55.74	53.83	100	3.20	3.22	6.6
	700	55.69	64.01	98.7	3.18	3.22	7.0
Ag^+/TiO_2	500	55.48	53.16	100	3.15	2.88	7.0
	700	50.82	53.80	98.8	3.15	2.92	7.3

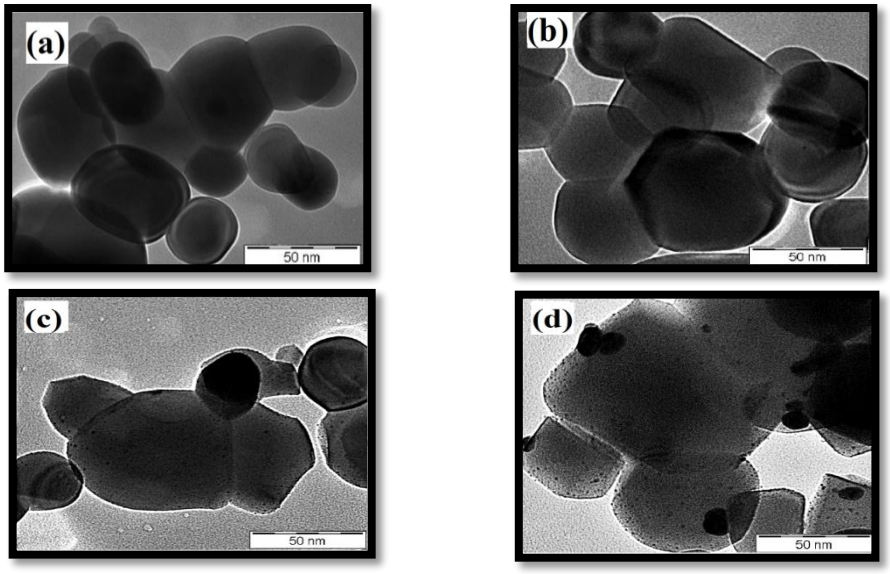

Fig. 2: TEM micrographs of TiO_2 calcined at (a) 500 °C, (b) 700 °C, and Ag^+ doped TiO_2 calcined at (c) 500 °C, (d) 700 °C, respectively.

energies (E_g) of pure and Ag^+ doped TiO_2 were calculated from the plot of $F(R)^2$ versus photon energy [E (eV)] for direct transition while for indirect transition, E_g were calculated from the plot of $F(R)^{1/2}$ versus E [19, 20], and the values are given in Table 1.

The calculated direct transition band gap energy (E_g) values are closer to the values reported in the literature (3.2 eV) for both pure and doped TiO_2. However, the indirect transition values for all Ag^+ doped TiO_2 samples were less than 3.2 eV (Table 3). The direct transition band gap energy value (≈3.2 eV) corresponding to the wavelength of 385 nm for the prepared pure TiO_2 sample is in close agreement with the previously reported values for the TiO_2 pure anatase phase [9, 18]. Meanwhile, the indirect transition band gap energy values were in the range of 2.88-2.95 eV corresponding to the wavelengths 440 and 415 nm for the samples calcined at 500 and 700 °C, respectively. The results predicted that anatase phase TiO_2 is an indirect bandgap semiconductor and follows the indirect transition of electrons [18].

The absorption edges for Ag^+ doped TiO_2 nanoparticles were dominant in the range of 405 to 430 nm, which indicated the shift towards the visible region, whereas the absorption wavelength of undoped samples was observed at less than 400 nm. An additional absorption peak corresponding to higher absorption in the visible region at 470 nm for Ag/TiO_2 nanoparticles calcined at 500 °C maybe associated with the enhanced photocatalytic activity of this material. The typical Ag nanoparticles plasmon absorption peak at 400 nm is responsible for the large shift due to the high refractive index of TiO_2 nanoparticles and the interaction between Ag metal and TiO_2 nanoparticles [28].

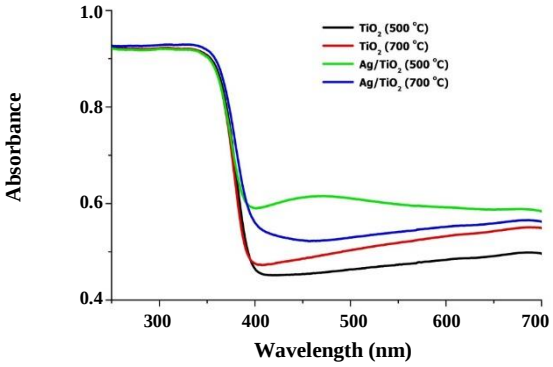

Fig. 3: DR UV-Vis absorption spectra of TiO_2 and Ag^+ doped TiO_2.

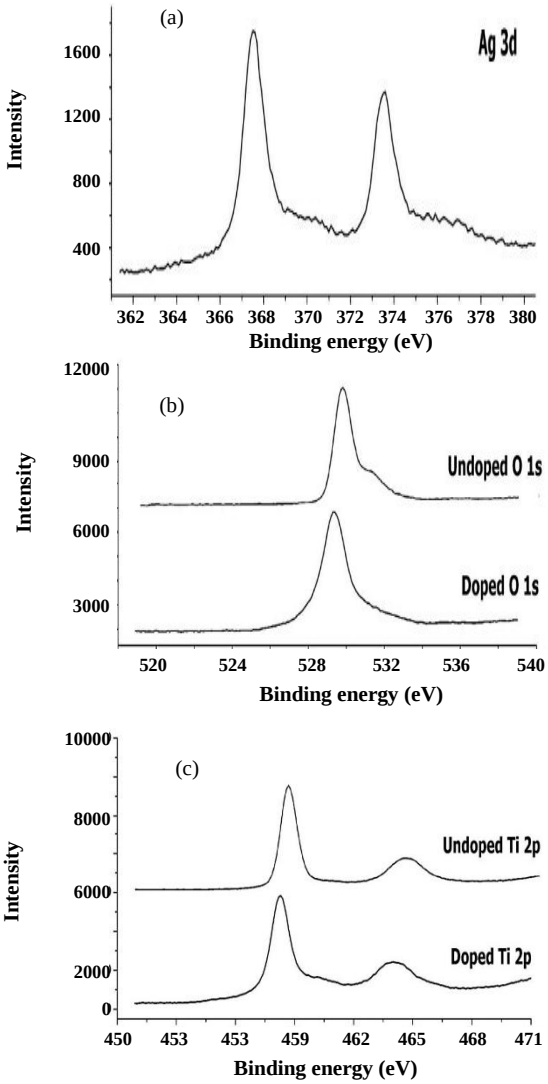

Fig. 4: The XPS spectra of the major peak for pure and Ag^+ doped TiO_2 NPs (a) Ag 3d, (b) O 1s, and (c) Ti 2p.

XPS Analysis

The chemical state and composition of pure and Ag/TiO_2 were investigated using X-ray Photoelectron Spectroscopy (XPS) and the results are shown in Fig. 4. The Ti $2p_{3/2}$ and Ti $2p_{1/2}$ peaks located at 459.4 and 465.1 eV, respectively, suggested that the predominant state of Ti element in the sample is Ti^{4+} [28]. However, it was observed that Ag-doped TiO_2, revealed with the shift in binding energy for Ti 2p to 458.8 and 464.5 eV respectively, for the characteristic Ti $2p_{3/2}$ and Ti $2p_{1/2}$ peaks.

The lower shift in binding energy can be associated with the strong interaction between Ag and defective site present on the surface of TiO_2, and the photo-generated excited electrons in TiO_2 transferred to Ag suggesting the transition of electrons to the conduction band [28]. Two characteristic photoelectron peaks at 367.4 and 373.8 eV are attributed to the Ag $3d_{5/2}$ and Ag $3d_{3/2}$ for silver ion (Ag^+). In a previous case [29], it has been reported that the chemical states of Ag in Ag-doped TiO_2 NPs exist mainly as Ag^0 (metallic Ag) and Ag^+ (Ag_2O) corresponding to the Ag $3d_{5/2}$ peaks at 368.2 and 367.6 eV, respectively. The present findings were in close agreement with the reported values of Ag^{2+} (AgO) in Ag-doped TiO_2 attributed to Ag $3d_{5/2}$ peak at 367.0 eV [29, 30]. The O 1s peak at 529.8 eV is assignable to the Ti-O bond. At high calcination temperatures, both pure and Ag^+ doped TiO_2 NPs did not show any sub-peak for O 1s associated with dissociated oxygen or hydroxyl-like groups on the surface of NPs.

the pH of the point of zero charge (pH_{pzc})

In heterogeneous photocatalysis, the charge associated with the surface functionality of metal oxides is an important characteristic. The selection of proper pH conditions in the removal of pollutants (whether anionic or cationic) can be drawn by knowing the surface charge of the photocatalyst. As well described, the pH at which the net surface charge of material is zero is considered as the pH_{PZC} of that material [31]. The pH_{PZC} of metal oxide nanoparticles mainly depends upon the factors such as chemical modifications of surface, particle size, and phase transformation [32, 33]. Fig. 5 illustrates the pH drift method results for pH_{PZC} of the pure and Ag-doped TiO_2 samples whereas the comparisons of values reported in literature and the current work are given in Table 1.

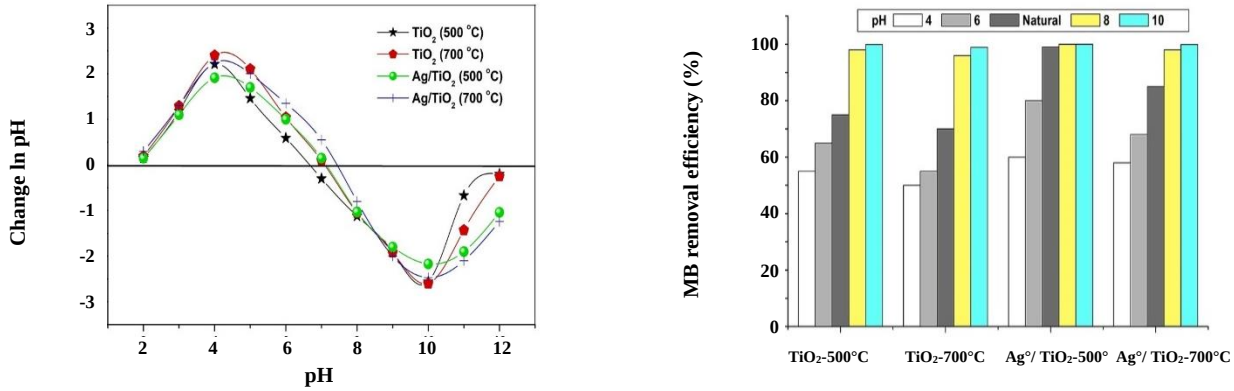

Fig. 5: Point of zero charge for (a) pure TiO_2 and (b) Ag-doped TiO_2 obtained using pH drift method and effects of different pH on the removal of MB.

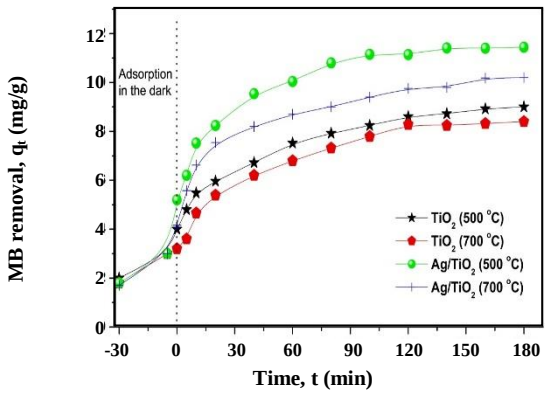

Fig. 6: Adsorption in the dark and removal efficiencies of undoped TiO_2 and Ag/TiO_2 calcined at various temperatures for MB degradation after 3 h under normal lab conditions.

Photocatalytic degradation of Methylene Blue (MB)

Equilibrium study

To verify the MB removal mechanism by pure and Ag^+ doped TiO_2 photocatalysts, some adsorption experiments were also conducted in the dark. The working solutions of MB (30 mg/L) were stirred in the dark using 0.2 g photocatalyst. It was observed that, in the absence of light, the amount of MB adsorbed for all the samples was very low. Pure and Ag-doped TiO_2 calcined at 500 °C showed slightly higher MB adsorption 4.9 and 5.7 %, respectively, after 180 min as compared to the samples calcined at 700 °C (Fig. 6).

In the meanwhile, the photocatalytic activities of pure and Ag^+ doped TiO_2 samples were also investigated for the degradation of MB under ordinary compact fluorescent light. No pH adjustment of analyte (MB solutions) was carried out and the experiments were conducted at pH (6.8±0.1) and temperature (25±2 °C). As can be seen that, the Ag/TiO_2 samples showed higher degradation efficiency as compared to the undoped TiO_2 prepared by the same method and treated at the same annealing temperatures (Fig. 6).

The Ag/TiO_2 sample calcined at 500 °C exhibited almost 100% MB degradation efficiency after 3 h. The results were consistent with the DR UV-Vis results showing a large absorption edge (> 400 nm) for Ag/TiO_2 (500 °C) in the visible region which is responsible for the enhanced degradation ability under visible light as compared to the undoped TiO_2.

Effects of competitive *ions (Cd^{2+}) on MB degradation*

The competitive degradation of MB using pure and Ag^+ doped NPs were tested in a binary solution of MB and Cd^{2+} with the concentration of each pollutant (200 mg/L). It was observed that the maximum MB degradation efficiencies (q_t, mg/g) of pure and Ag-doped TiO_2 enhanced approximately 4-4.5 folds in the presence of Cd^{2+} ions. Table 2 illustrates the maximum degradation efficiencies by pure and Ag^+ doped TiO_2 in the presence and absence of Cd^{2+} ion in comparison with different reported adsorbents as well as with and without competitive ions as examined in the present work. The enhanced efficiencies of TiO_2 NPs can probably support that the degradation of MB involved in the removal mechanism. The presence of cations (i.e. Cd^{2+}) in the solutions can effectively trap the photo-generated electrons and thus prolong the lifetime of photo-generated charge which leads to the enhanced degradation of MB.

Table 2: Comparative MB adsorption capacities of different adsorbents.

Adsorbents	Adsorption capacity of MB (30 mg/L), q_t (mg/g)	Adsorption capacity of MB (200 mg/L), q_t (mg/g) in presence of $Cd^{2+,*}$	Ref
Apricot stones-activated carbon 750 ºC	4.11		[34]
Walnut shell-activated carbon 750 ºC	3.53		
Almond shell-activated carbon 750 ºC	1.33		
Coal fly ash (0.01M NaCl)	16.60		[35]
Coal fly ash	12.70		
Raw beach sawdust	9.78		[36]
Zeolite	4.47		[37]
Zeolite based TiO_2 (UV-irradiation)	8.00		
TiO_2 loaded cashew nut shell activated carbon	4.81		[38]
TiO_2 (500 ºC)	9.00	36.00	This work
TiO_2 (700 ºC)	8.40	34.00	
Ag/TiO_2 (500 ºC)	11.40	46.00	
Ag/TiO_2 (700 ºC)	10.20	42.00	
$^{*}[Cd^{2+}]_o$ = 200 mg/L			

These results corroborate that, although Ag^+ dopant reduces the electron-hole pair recombination to significant values there is still the chance of de-excitation of photo-generated charge. The enhanced photo activities of Ag^+ doped NPs in the presence of competitive ions verify this assumption.

The mechanism of MB degradation by using as prepared undoped/pure and Ag^+ doped TiO_2 in the presence of an electron trapper, Cd^{2+} ions can be evaluated successfully. The findings have shown that the presence of Cd^{2+} ions effectively enhance the MB degradation up to four folds for all the synthesized samples (Table 2). The maximum degradation efficiency of Ag^+ doped TiO_2 calcined at 500 °C was found to be q_t = 46 mg/g, which is comparatively higher than without electron trap agent (11.4 mg/g), under the same set of experimental conditions. The results obtained supported the effective role of photo-generated valence band hole in the degradation of MB in the presence of electron trapper ions.

The selected results of EDX and XRF analyses of fresh and spent pure and Ag^+ doped TiO_2 samples calcined at 500 °C are tabulated in Table 3. No trace of residual nitrogen from the nitrate-containing metal precursor was observed on the surface of any Ag-doped TiO_2 NPs indicating that with high annealing temperature the nitrogen contents escaped in the form of oxides [39]. The surface contents observed by EDX analyses of pure and Ag-doped TiO_2 showed major component of TiO_2 (~97 mass %), whereas the XRF results of fresh and spent photocatalyst showed a minute concentration of C and S as well. However, the presence of C and S are not sufficient to verify the presence of any adsorbed MB or degradation products. The EDX results of spent samples did not show any trace residue of nitrogen or sulfur, however, there is some carbon content present in fresh and used samples which may be due to the adhesive carbon tape used during EDX sample preparations.

Regeneration study

The regeneration studies of spent pure and Ag-doped photocatalysts were also conducted by using a high-temperature combustion method for the removal of 30 mg/L MB solution and the results are shown in Fig 7. It can be seen that the performance of regenerated samples in the 2nd and 3rd cycles decreased only up to 10%. The regeneration by the high-temperature combustion method was found more effective for the reuse of TiO_2 photocatalysts as compared to the chemically regenerated photocatalyst (i.e. using the Fenton oxidation process).

Table 3: Elemental composition of fresh and spent pure and Ag-doped TiO_2 photocatalyst calcined at 500 °C obtained from EDX and XRF analyses.

Nanoparticles	EDX mass (%)					XRF mass (%)				
	Ti	O	Ag	C	S	Ti	O	Ag	C	S
TiO_2 (fresh)	52.00	45.40	-	2.64	-	56.30	42.50	-	0.73	0.006
TiO_2 (used)	50.10	46.80	-	3.13	-	58.40	40.40	-	0.67	0.005
Ag/TiO_2 (fresh)	56.50	40.20	1.01	2.21	-	57.10	40.30	1.38	0.75	0.016
Ag/TiO_2 (used)	46.20	49.10	0.85	3.56	-	56.80	40.60	1.21	0.82	0.014

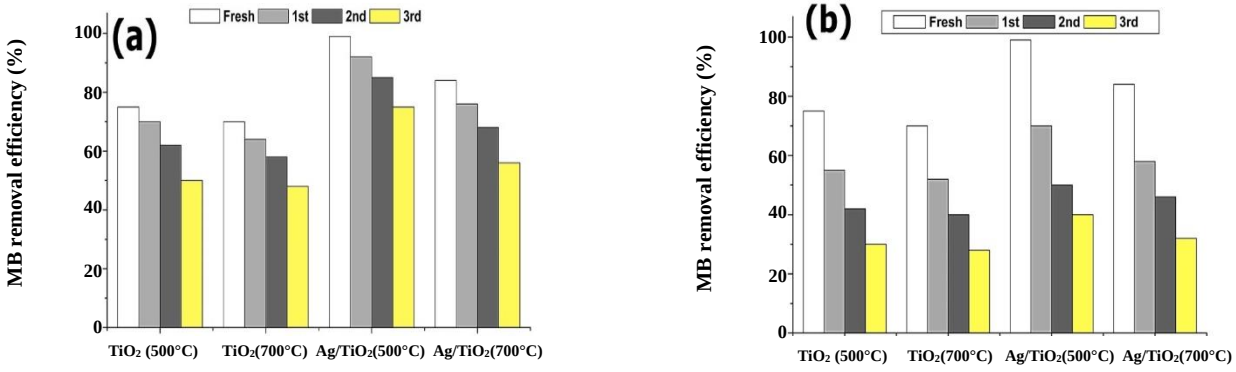

Fig. 7: Comparison of MB removal efficiency (%) of fresh and (a) high-temperature combustion, and (b) Fenton oxidations regenerated TiO_2 and Ag-doped TiO_2, respectively.

It is expected that during physical regeneration involving high temperature the spent nanoparticles regain the active surface while the traces residue of MB may cause some synergistic/doping effect with undoped and Ag-doped TiO_2. In the Fenton oxidation process, Fe ions from the regeneration solution can be adsorbed on the surface or penetrate into the pores of solid adsorbents, which reduces the ion exchange capacity of regenerated samples for re-absorption [22]. Similarly, the large amount of water adsorbed by the photocatalyst during the reaction in the aqueous medium may cause a reduction in crystallinity and loss of active surface areas due to the aggregations of nanoparticles.

CONCLUSIONS

The doping of silver as Ag^+ ion into TiO_2 surface enhanced the photocatalytic efficiency under ordinary compact fluorescent light and ambient conditions and also helped in reducing the electron/hole pair recombination rate. The anatase phase was dominant as revealed by the XRD results. A significant decrease in the bandgap from 3.20 to 2.88 eV was observed for the Ag^+ doped TiO_2 sample calcined at 500 °C. Almost complete MB degradation for the Ag-doped TiO_2 calcined at 500 °C was obtained without UV irradiation. The addition of a photo-generated electrons trapper (Cd^{2+}) significantly improved the lifetime of photo-generated charge (electron-hole pairs) resulting in the enhanced photo-degradation of MB (q_t = 34-46 mg/g) under ambient conditions. EDX, XRF, and XPS analyses for both the fresh and used photocatalysts indicated the photocatalytic MB degradation. The regeneration study indicates that physical regeneration is more significant for the reutilization of photocatalysts as compared to the Fenton oxidation.

Acknowledgments

The authors greatly acknowledge the financial support by Universiti Sains Malaysia (USM) under the RUI Grant No. 1001/PKIMIA/815099. NS is also thankful to The World Academy of Sciences (TWAS) and USM for awarding the TWAS–USM Fellowship to pursue this study.

Received : Oct. 14, 2019 ; Accepted : May 4, 2020

REFERENCES

[1] Ogugbue, C.J., Sawidis, T., Bioremediation and Detoxification of Synthetic Wastewater Containing Triarylmethane Dyes by Aeromonas Hydrophila Isolated from Industrial Effluent, *Biotechnol. Res. Int.*, **2011***:* (2011).

[2] Wu, J., Doan, H., Upreti, S., Decolorization of Aqueous Textile Reactive Dye by Ozone, *Chem. Eng. J.*, **142**: 156-160 (2008).

[3] Mahdavi, S., Nano-TiO_2 Modified With Natural and Chemical Compounds as Efficient Adsorbents for the Removal of Cd^{+2}, Cu^{+2}, and Ni^{+2} from Water, *Clean Technol. Environ. Policy*., **18**: 81-94 (2016).

[4] Jalbani N., Soylak M., Ligandless Surfactant Mediated Solid Phase Extraction Combined with Fe_3O_4 Nano-Particle for the Preconcentration and Determination of Cadmium and Lead In Water and Soil Samples Followed By Flame Atomic Absorption Spectrometry: Multivariate Strategy, *Ecotoxicol. Environ. Safty.*, **102**: 174-178 (2014).

[5] EPA. 2011. "Edition of the Drinking Water Standards and Health Advisories." EPA 820-R-11-002, Office of Water, Washington (DC): The United States Environmental Protection Agency; (2011).

[6] Huang, H.H., Tseng, D.H., Juang, L.C., Titanium Dioxide Mediated Photocatalytic Degradation of Monochlorobenzene in Aqueous Phase, *Chemosphere*, **71**: 398-405 (2008).

[7] Thiruvenkatachari, R., Vigneswaran, S., Moon, I.S., A Review on UV/TiO_2 Photocatalytic Oxidation Process, *Kor. J. Chem. Eng.*, **25**: 64-72 (2008).

[8] Janitabar Darzi, S., Abdolmohammadi, S., Latifi, M., Green Removal of Toxic Th(IV) by Amino-Functionalized Mesoporous TiO_2-SiO_2 Nanocomposite, *Iran. J. Chem. Chem. Eng. (IJCCE)*, **39(2)**: 101-202 (2020).

[9] Saqib, N.U., Adnan, R., Shah, I., Zeolite Supported TiO_2 with Enhanced Degradation Efficiency for Organic Dye Under Household Compact Fluorescent Light, *Mate. Res. Express*, **6(9)**: 095506 (2019).

[10] Chan S.H.S., Yeong W.T., Juan J.C., Teh C.Y., Recent Developments of Metal Oxide Semiconductors as Photocatalysts in Advanced Oxidation Processes (AOPs) for Treatment of Dye Waste-Water, *J. Chem. Technol. Biotechnol.*, **86**: 1130-1158 (2011).

[11] Ramacharyulu P., Kumar, J.P., Prasad, J.K., Sreedhar, B., Sulphur Doped Nano TiO_2: Synthesis, Characterization and Photocatalytic Degradation of a Toxic Chemical in Presence of Sunlight, *Mater. Chem. Phys*, **148**: 692-698 (2014).

[12] Vasili R., Stojadinovi S., Radi N., Stefano, P., Dohcevic-Mitrovi Z., Grbi B., One-Step Preparation and Photocatalytic Performance of Vanadium Doped TiO_2 Coatings, *Mater. Chem. Phys.*, **151**, 337-344 (2015).

[13] Palukuru P.S., Devangam A V. Behara D.K., N, S-Codoped TiO_2/Fe_2O_3 Heterostructure Assemblies for Electrochemical Degradation of Crystal Violet Dye, *Iran. J. Chem. Chem. Eng. (IJCCE)*, **39(2)**: 171-180 (2018).

[14] Saqib N.U., Adnan R., Shah I., A Mini-Review on Rare Earth Metal-Doped TiO_2 for Photocatalytic Remediation of Wastewater, *Environ. Sci. Pollut. Res.*, **23(16)**: 15941-15951 (2016).

[15] Chowdhury, P., Moreira, J., Gomaa, H., Ray, A.K., Visible-Solar-Light-Driven Photocatalytic Degradation of Phenol with Dye-Sensitized TiO_2: Parametric and Kinetic Study, *Ind. Eng. Chem. Res.*, **51**: 4523-4532 (2012).

[16] Daghrir, R., Drogui, P., Robert, D., Modified TiO_2 for Environmental Photocatalytic Applications: A Review, *Ind. Eng. Chem. Res*, **51**: 3581-3599 (2013).

[17] Janusz, W., Matysek, M., Coadsorption of Cd (II) and Oxalate Ions at the TiO_2/Electrolyte Solution Interface, *J. Colloid Interface Sci.*, **296**: 22-29 (2006).

[18] Saqib, N.U., Adnan, R., Shah, I., Modifications of Pure and Ag Doped TiO_2 by Pre-Sulphated and Calcination Temperature Treatments, *Res. Chem. Intermed*, **43(11)**: 6571-6588 (2017).

[19] Liu G.L., Zhu D.W., Liao S.J., Ren L.Y., Cui J.Z., Zhou W.B., Solid-Phase Photocatalytic Degradation of Polyethylene–Goethite Composite Film under UV-Light Irradiation, *J. Hazard. Mater*, **172**: 1424-1429 (2009).

[20] Gaya U.I., Comparative Analysis of ZnO-Catalyzed Photo-Oxidation of p-Chlorophenols, *Chem. Eur. J.*, **2**: 163-167 (2011).

[21] Yang Y., Chun Y., Sheng G., Huang M., pH-Dependence of Pesticide Adsorption by Wheat-Residue-Derived Black Carbon, *Langmuir*, **20**: 6736-6741 (2004).

[22] Wang S., Li H., Xie S., Liu S., Xu L., Physical and Chemical Regeneration of Zeolitic Adsorbents for Dye Removal in Wastewater Treatment, *Chemosphere*, **65**: 82-87 (2006).

[23] Uzunova-Bujnova M., Todorovska R., Dimitrov D., Todorovsky D., Lanthanide-Doped Titanium Dioxide Layers as Photocatalysts, *Appl. Surf. Sci.*, **254(22)**: 7296-302 (2008).

[24] Szabó-Bárdos E., Czili H., Horváth A., Photocatalytic Oxidation of Oxalic Acid Enhanced by Silver Deposition on a TiO_2 Surface, *J. Photochem. Photobiol. A: Chemistry*, **154(2)**: 195-201 (2003).

[25] Li X., Wang L., Lu X., Preparation of Silver-Modified TiO_2 *via* Microwave-Assisted Method and Its Photocatalytic Activity for Toluene Degradation, *J. Hazard. Mater*, **177**: 639-647 (2010).

[26] Ahmad A., Thiel J., Shah S.I., Structural Effects of Niobium and Silver Doping on Titanium Dioxide Nanoparticles, *J. Phys.*, Conference Series, **61**: 11 (2007).

[27] Chao H., Yun Y., Xingfang H., Larbot A., Effect of Silver Doping on the Phase Transformation and Grain Growth of Sol-Gel Titania Powder, *J. Eur. Ceram. Soc*, **23(9)**: 1457-1464 (2003).

[28] Demirci S., T. Dikici, M., Yurddaskal S., Gultekin M., Toparli., Celik E., Synthesis and Characterization of Ag Doped TiO_2 Heterojunction Films and their Photocatalytic Performances, *App. Surf. Sci*, **390**: 591-601 (2016).

[29] Feng N., Wang Q., Zheng A., Zhang Z., Fan J., Liu S.B., Amoureux J.P., Deng F., Understanding the High Photocatalytic Activity of (B, Ag)-Codoped TiO_2 under Solar-Light Irradiation with XPS, Solid-State NMR, and DFT Calculations, *J. American Chem. Society*, **135(4)**: 1607-1616 (2013).

[30] Taing J., Cheng M.H., Hemminger J.C., Photodeposition of Ag or Pt onto TiO_2 Nanoparticles Decorated on Step Edges Of HOPG, *ACS Nano*, **5(8)**: 6325-6333 (2011).

[31] Hotze E.M., Phenrat T., Lowry G.V., Nanoparticle Aggregation: Challenges to Understanding Transport and Reactivity in the Environment, *J. Environ. Qual*, **39**: 1909-1924 (2010).

[32] Lin D., Tin X., Wu F., Xing B., Fate and Transport of Engineered Nanomaterials in the Environment, *J. Environ. Qual*, **39**: 1896-1908 (2010).

[33] Dutta P.K., Ray A.K., Sharma V.K., Millero F.J., Adsorption of Arsenate and Arsenite on Titanium Dioxide Suspensions, *J. Colloid. Interface. Sci.*, **278**: p. 270-275 (2004).

[34] Aygün A., Yenisoy-Karakaş S., Duman I., Production of Granular Activated Carbon from Fruit Stones and Nutshells and Evaluation of Their Physical, Chemical and Adsorption Properties, *Micropor. Mesopor. Mater*, **66(2-3)**: 189-195 (2003).

[35] Wang S., Ma Q., Zhu Z., Characteristics of Coal Fly Ash and Adsorption Application, *Fuel*, **87(15)**: 3469-3473 (2008).

[36] Batzias, F., Sidiras, D., Dye Adsorption by Calcium Chloride Treated Beech Sawdust In Batch and Fixed-Bed Systems, *J. Hazard. Mater*, **114(1)**: 167-174 (2004).

[37] Faghihian, H., Bahranifard, A., Application of TiO_2–Zeolite as Photocatalyst for Photodegradation of Some Organic Pollutants, *Iranian J. Catal*, **1(1)**: p. 45-50 (2011).

[38] Ragupathy, S., Raghu, K., Prabu, P., Synthesis and Characterization of TiO_2 Loaded Cashew Nut Shell Activated Carbon and Photocatalytic Activity on BG and MB Dyes Under Sunlight Radiation, *Spectrochimica Acta Part A: Molecular and Biomolecular Spectroscopy*, **138**: 314-320 (2015).

[39] Maicu M., Hidalgo M.C., Colon G., Navio J.A., Comparative Study of the Photodeposition of Pt, Au and Pd on Pre-Slphated TiO_2 for the Photocatalytic Decomposition of Phenol, *J. Photochem. Photobiol. A: Chem.*, **217**: 275-283 (2011).